BeatProfiler: Multimodal In Vitro Analysis of Cardiac Function Enables Machine Learning Classification of Diseases and Drugs

Youngbin Kim ⓘ *, Member, IEEE*, Kunlun Wang ⓘ, Roberta I. Lock, Trevor R. Nash ⓘ, Sharon Fleischer ⓘ, Bryan Z. Wang ⓘ, Barry M. Fine, and Gordana Vunjak-Novakovic ⓘ

Abstract—Goal: **Contractile response and calcium handling are central to understanding cardiac function and physiology, yet existing methods of analysis to quantify these metrics are often time-consuming, prone to mistakes, or require specialized equipment/license. We developed BeatProfiler, a suite of cardiac analysis tools designed to quantify contractile function, calcium handling, and force generation for multiple in vitro cardiac models and apply downstream machine learning methods for deep phenotyping and classification.** *Methods:* **We first validate BeatProfiler's accuracy, robustness, and speed by benchmarking against existing tools with a fixed dataset. We further confirm its ability to robustly characterize disease and dose-dependent drug response. We then demonstrate that the data acquired by our automatic acquisition pipeline can be further harnessed for machine learning (ML) analysis to phenotype a disease model of restrictive cardiomyopathy and profile cardioactive drug functional response. To accurately classify between these biological signals, we apply feature-based ML and deep learning models (temporal convolutional-bidirectional long short-term memory model or TCN-BiLSTM).** *Results:* **Benchmarking against existing tools revealed that BeatProfiler detected and analyzed contraction and calcium signals better than existing tools through improved sensitivity in low signal data, reduction in false positives, and analysis speed increase by 7 to 50-fold. Of signals accurately detected by published methods (PMs), BeatProfiler's extracted features showed high correlations to PMs, confirming that it is reliable and consistent with PMs. The features extracted by BeatProfiler classified restrictive cardiomyopathy cardiomyocytes from isogenic healthy controls with 98% accuracy and identified relax90 as a top distinguishing feature in congruence with previous findings. We also show that our TCN-BiLSTM model was able to classify drug-free control and 4 cardiac drugs with different mechanisms of action at 96% accuracy. We further apply Grad-CAM on our convolution-based models to identify signature regions of perturbations by these drugs in calcium signals.** *Conclusions:* **We anticipate that the capabilities of BeatProfiler will help advance in vitro studies in cardiac biology through rapid phenotyping, revealing mechanisms underlying cardiac health and disease, and enabling objective classification of cardiac disease and responses to drugs.**

Index Terms—Calcium handling, cardiac analysis, contractile function, drug response, machine learning (ML).

Impact Statement— BeatProfiler rapidly quantifies contractile function and calcium handling of in vitro cardiac models enabling ML classification of cardiac disease and cardioactive drugs.

I. INTRODUCTION

THE ability to reliably assess cardiac function using in vitro models is crucial in modeling functional decline associated with cardiac injury, disentangling elements of genetic or complex multifactorial diseases, and effectively evaluating cardioprotective drug response [1]. Cardiomyocyte function is evaluated in vitro from traces of cardiac contractions obtained from brightfield and phase-contrast videos and calcium signals using ion-sensitive dyes and genetic reporters [2], [3]. To extract metrics that reflect functional changes accompanying a disease or drug exposure in a fast, reliable, and unbiased manner, calcium and contractile videos must be further processed (Fig. 1(a)).

Existing methods have significant limitations that hinder typical biomedical researchers from using them (Table S1-3) [4], [5], [6], [7], [8], [9], [10], [11]. There is no single software that can analyze both contractile and calcium handling functions through consolidation of multimodal analysis into a singular integrated tool. They are often dependent on external programs such as ImageJ or MATLAB, requiring additional setup. Analysis with
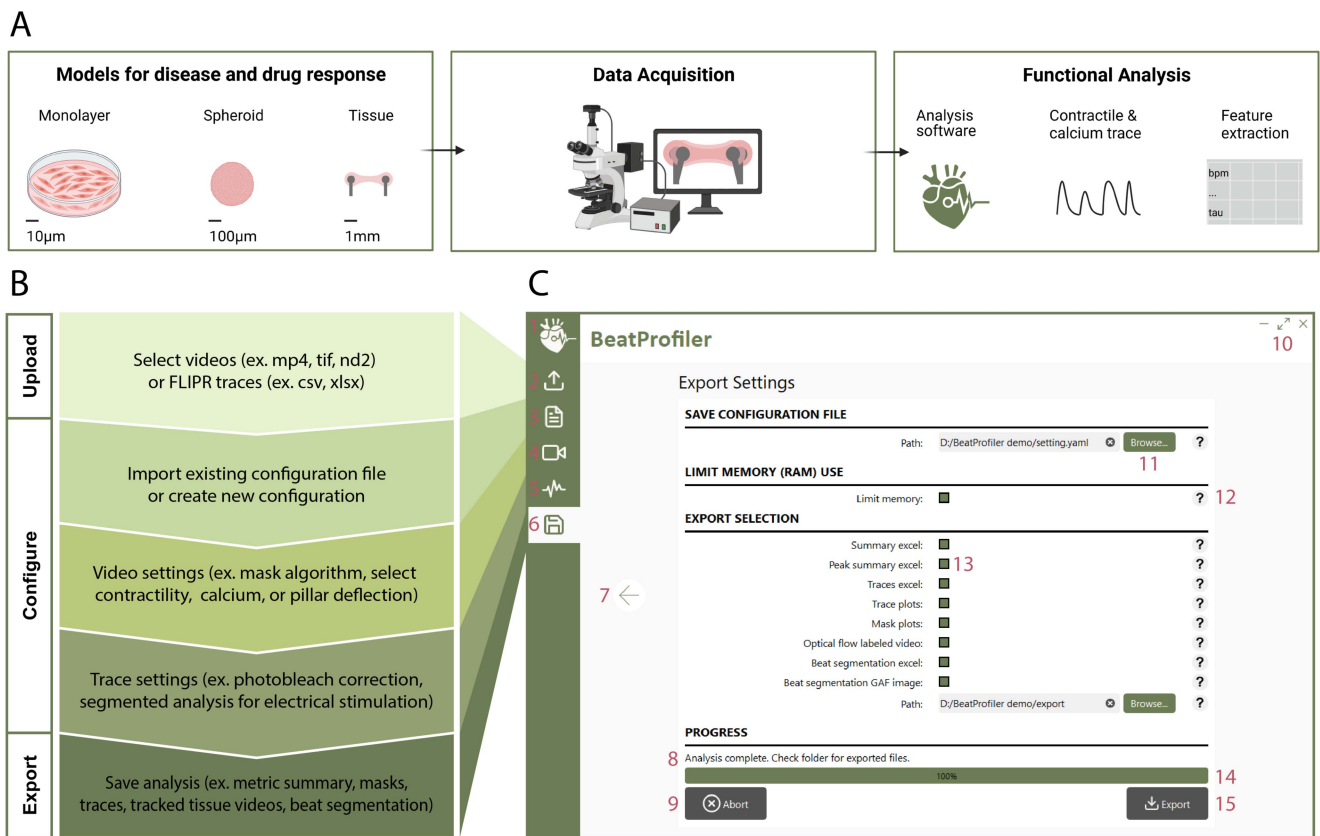
Fig. 1. Study Overview and BeatProfiler pipeline. (a) In vitro cardiac functional analysis workflow. (b) BeatProfiler analysis pipeline. Upload data, configure settings, and export analysis (top to bottom). (c) BeatProfiler graphical user interface at the export page. Components are labeled as follows: 1) home 2) upload 3) configuration 4) video settings 5) trace settings 6) export 7) previous page 8) progress message 9) abort analysis 10) min, max, close 11) file browse 12) help 13) toggle selection 14) progress bar 15) analyze and export.

these methods often requires manual parameter inputs, hindering high throughput analysis. Many methods are sensitive to noise and artifacts, preventing accurate analysis in low-signal videos. Compatibility with various file types can pose problems for previous methods that are limited to a single or a few file types. The lack of automated mask identification for many of these methods results in low-quality signals. Lastly, many existing methods are either proprietary or deprecated and no longer available online.

BeatProfiler was designed to overcome limitations of existing methods by: i) accurate analysis of multimodal data (brightfield and fluorescent videos), ii) assessment of different in vitro models (i.e., monolayer, cardiac spheroid, engineered tissue), iii) software integration into a fully automated pipeline to avoid user bias and improve reproducibility, iv) data preparation and preprocessing for ML applications, v) scalable near real-time compute to enable high throughput analysis, and vi) provision of an interactive, user-friendly GUI (Fig. 1(b) and (c)).

There is also a need to facilitate ML applications to obtain more meaningful information from complex functional data, as evidenced by its utilization in drug discovery, medical diagnostics, protein design, and sequencing analysis [12], [13], [14], [15], [16], [17]. Several groups have applied traditional ML to classify contractile and calcium responses of healthy and diseased cardiomyocytes [18], [19], [20] and cardiac drug

responses in vitro [21], [22]. However, these approaches have mostly been restricted to feature-based ML, which is limited by predefined parameters extracted from the original contractile or calcium time series. These parameters may be sufficient in simple tasks, as demonstrated in our restrictive cardiomyopathy disease classification, but they fail in more complex problems due to suboptimal and/or biased feature selection. Deep learning, which can overcome these limitations, has only been applied in a few binary classifications of induced pluripotent stem cell derived cardiomyocytes (iPS-CMs) [23]. As predicting cardioactivity in preclinical models is of great interest for drug development, we demonstrate the application of deep learning beyond simple binary classification in classification of four drugs based on their mechanisms of action with drug-free control cardiomyocytes. We then applied gradient-weighted class activation mapping (Grad-CAM) in our drug classification tasks to gain insight into convolution-based deep learning models and validate our model on drugs with known effects.

We have developed BeatProfiler to address the need for a unified, user-friendly program to rapidly process large multimodal datasets of in vitro cardiac models such as monolayers, cardiac spheroids, and engineered tissues. BeatProfiler is a versatile software platform capable of analyzing videos in many formats (tif, mp4, mov, nd2, etc.) as well as contractile or calcium traces in Excel format, with capability to extract features, segment

single beats, and prepare data for further ML analysis. We first validate BeatProfiler against existing standards and confirm its ability to detect changes from disease and drugs. We then profile healthy iPS-CM and isogenic iPS-CM with restrictive cardiomyopathy-causing variant using an existing dataset [24] and classify them by ML using functional cell responses. We further substantiate the capabilities of BeatProfiler and the related automated data acquisition pipeline in a proof-of-concept study of classifying cardioactive drugs by their mechanism of action using ML (Fig. S2A). Using Grad-CAM, we validate our models by highlighting important regions involved in their predictions. We illustrate the modularity of our tools through analysis of different data modalities within high-throughput contexts. Our data acquisition, analysis, and ML pipeline enable deeper insight into in vitro cardiac models, facilitating a more comprehensive understanding of functional impacts of disease and aiding in developing novel therapeutics.

II. Materials and Methods

A. BeatProfiler Development

BeatProfiler was implemented in Python 3 with dependencies including NumPy, SciPy, pandas, scikit-learn, matplotlib, FFmpeg, nd2reader, PySide2, and PyTorch. The BeatProfiler library is available as a pip package for direct use in Python. The GUI wrapper was designed using QT Designer and packaged into a Windows and MacOS software using PyInstaller.

B. Automated Pillar Identification Through Deep Learning Object Detection

An object detection model based on YOLOv8 architecture was trained to identify two pillar heads present in each image. To automatically detect pillar heads in the milliPillar platform, we trained an object detection algorithm, YOLOv8 [25]. 1532 images were manually labeled and split into train, validation, and test sets at 70:20:10 ratio. Each training image was randomly augmented three times by flipping, rotating, changing brightness, changing saturation, and Gaussian blurring to artificially generate more samples.

We evaluated the model against a previously unseen dataset, achieving mean average precision (mAP) score of 0.993 when tested at intersection over union (IOU) threshold of 0.5, as measured by area under the precision-recall curve (Fig. S1B).

C. Automated Tissue Width Measurement Through Deep Learning Segmentation

A YOLOv8 instance segmentation model was trained to segment pixels belonging to the tissue (Fig. 2(k)). We manually labeled 737 tissues to train a segmentation algorithm using YOLOv8. The same split ratio was used as above for train, validation, and test sets with the same random augmentations. The mask segmentation was used to automatically determine tissue widths for milliPillar tissues by measuring the distance of the line within the mask perpendicular to the line connecting the centers of each pillar head and crossing the midpoint between the centers as detected by the previous algorithm.

From the segmentation mask, tissue width was determined at the midpoint between the two pillar heads identified by the previous model. When validated against a previously unseen test set, the segmentation algorithm had an mAP of 0.995 at IOU threshold of 0.5 (Fig. S1B).

D. Datasets

We acquired $FLNC^{\Delta GAA}$, $FLNC^{\Psi WT}$, and $GCaMP^{\Delta GAA}$, $GCaMP^{\Psi WT}$ data through our previously published study [24]. Dataset for drug classification was acquired as described in the automated data acquisition section in the supplementary.

Each dataset was filtered to drop low-quality samples by discarding samples with bpm < 20 (slow beating), SDRR > 0.7 (irregular beating/noise), and amplitude > 1 (imaging artifact).

For disease classification, the dataset (n=352 for ΨWT and n=296 for ΔGAA) was stratified based on the label and randomly split into train and test sets at 85:15 ratio. We took 25 features extracted from each sample and normalized each feature to have mean of 0 and standard deviation of 1 to use as input for each model.

Videos for drug studies were analyzed through BeatProfiler to generate three input datasets for machine learning: feature summary (tabular), photobleach corrected single beat segments (time series), and Gramian angular field (image) of time series. Following single-beat segmentation, the data was processed to ensure the same input dimension size of 200. Longer segments were truncated to fit within the length, and shorter segments were padded with the last value of the segment. Resulting beats were transformed through Gramian angular field (GAF) to generate one image per beat. Additional information on the number of data points and splits across classes are in the supplementary.

Additional information about cell culture, drug studies, data acquisition, and data processing is found in supplementary information. A list of all data used in this paper is outlined in Table S4.

E. Statistical Analysis

The sample size for each experiment is denoted in the figure descriptions. Statistical analysis was performed with Prism 9. Student's t-test was used to analyze two unpaired groups, and one-way analysis of variance (ANOVA) with Tukey post hoc test was used to compare more than two groups. Significance asterisks denote the following: n.s.: $p > 0.05$, *: $p \leq 0.05$, **: $p \leq 0.01$, ***: $p \leq 0.001$, and ****: $p \leq 0.0001$. Error bars in all figures denote standard deviation.

III. Results

A. BeatProfiler Analysis Pipeline

BeatProfiler was developed to analyze cardiac traces, segment single beats, and assess functional features using brightfield and fluorescent videos of *monolayers, spheroids,* and *tissues*. It enables quantitative profiling of cardiac function in three modalities: *contractility, calcium handling,* and *tissue pillar*
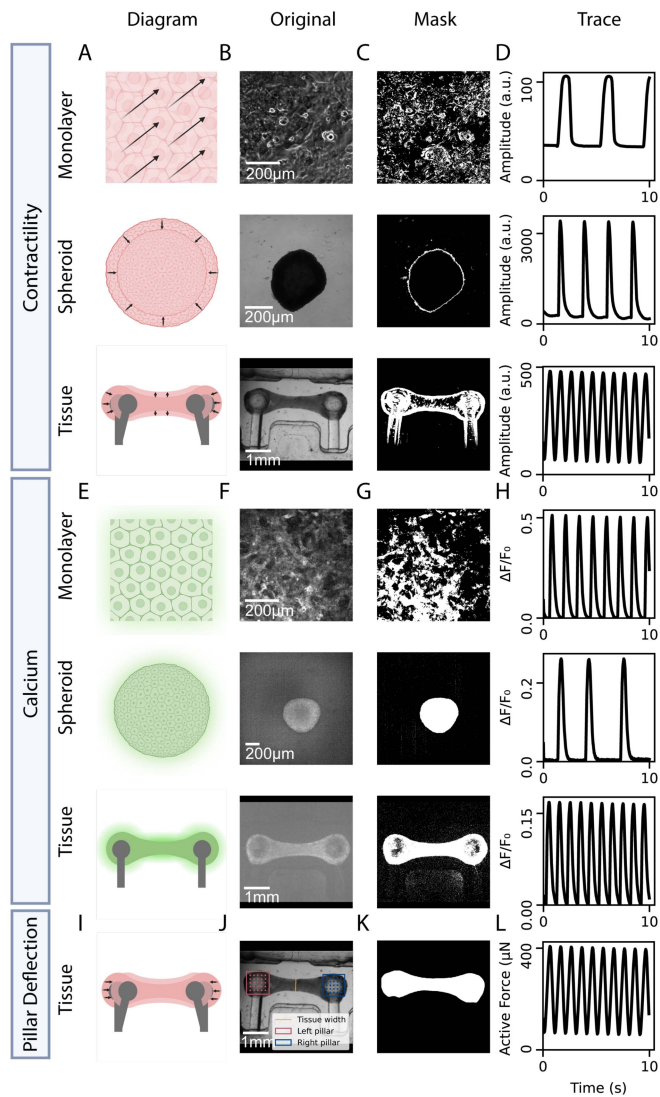
Fig. 2. BeatProfiler analyzes contractile function, calcium handling, and pillar deflection. From top to bottom: Diagram and analysis pipeline for brightfield contractility, calcium handling, and pillar deflection in order of monolayer, spheroid, and engineered tissue. (a) Graphical representation of contractility measurements. (c) Representative frames extracted from contractility videos. (c) ROI mask generated for each biological model. (d) Contractility traces for each biological model. (e) Graphical representation of calcium transient measurements. (f) Representative frames extracted from calcium videos. (g) ROI mask generated for each biological model. (h) Calcium traces for each biological model. (i) Graphical representation of pillar deflection measurements. The left and right pillars and tissue width were automatically identified by deep learning. Points for each pillar were used to track pillar deflection over time. (j) Representative frames extracted from a pillar deflection video for an engineered tissue. (k) ROI mask generated with deep learning. (l) Active force trace derived from pillar deflection.

deflection–uniaxial deflection of pillars to which tissues are attached.

The first modality, *contractility*, processes brightfield or phase contrast videos to quantify omnidirectional cardiomyocyte contraction (Fig. 2(a)). This method quantifies beating of monolayers, spheroids, and engineered tissues in a direction-agnostic manner, enabling analysis regardless of beating orientation (uniaxial, multiaxial, or radial) (Fig. 2(b)). Masks are automatically

calculated to identify regions of interest (ROI), as described further in supplementary (Fig. 2(c)). Using the principle of pixel intensity differences in reference to video frames at the relaxed state, the contractile time series is extracted from the masked video (Fig. 2(d)).

The second modality, *calcium handling*, analyzes calcium transients by tracking pixel intensity over time (Fig. 2(e)). Also compatible with 2D or 3D biological models (Fig. 2(f)), this modality automatically masks ROI using the same principles outlined above (Fig. 2(g)). In calcium imaging, a common phenomenon is photobleaching, in which baseline fluorescent intensity decays over time (Fig. S1A). To correct for this effect, BeatProfiler is optimized to automatically impute the changing baseline fluorophore decay (F_0) (Fig. 2(h)).

The last modality, *tissue pillar deflection*, also analyzes brightfield or phase contrast contractile videos. In this case, uniaxial contractile force generated by engineered tissues is quantified (Fig. 2(i)) by optical flow tracking of pillars displaced by force exerted by the attached tissue. To enable this analysis, users define two regions on the pillars to track over time. Within the specified regions, a fixed set of points is selected to track over time (Fig. 2(j)). Distance between the two pillars is computed after discarding poorly tracked points (Movie S1) [26]. The pillar displacement is translated to force if the user provides the displacement-force relationship determined by the tissue platform's mechanical properties (Fig. 2(l)). Tissue stress, defined as the force divided by tissue cross-sectional area, is calculated using tissue width assuming that tissue cross-sections are circular. This semi-automated approach is compatible with most engineered tissue platforms, requiring user-labeled pillars and tissue widths.

To expedite the analysis and reduce potential bias, we sought to fully automate pillar detection and tissue width measurements for one particular setting, the milliPillar platform [9], which was previously developed and characterized in our lab. We achieved this using two deep learning models with YOLOv8 architecture, which are described in supplemental materials. Notably, manual pillar distance and tissue width measurements compared to BeatProfiler's deep learning based measurements show high correlation coefficients of $R^2 = 0.935$ and $R^2 = 0.973$, respectively (Fig. S1C). Automated measurements of these two parameters enabled complete end-to-end analysis for milliPillar tissues from video to final output.

BeatProfiler can process extracted traces according to user-defined configurations and create an export folder in a specified directory containing output files. The outputs include contractile, calcium, force, stress, displacement traces, and single-beat segmentations from each video. Functional metrics describing beat frequency, velocity, contraction time, and relaxation time are exported for individual beats and summarized at the sample level (Fig. S1D, Table S5). Additionally, BeatProfiler quantifies force and stress generated by tissues for the pillar deflection modality (Fig. S1E). Images of traces and masks are exported for easy quality control. Segmented individual beats transformed through Gramian angular field, a method for representing time series data in image formats, are also exported for further deep learning applications.
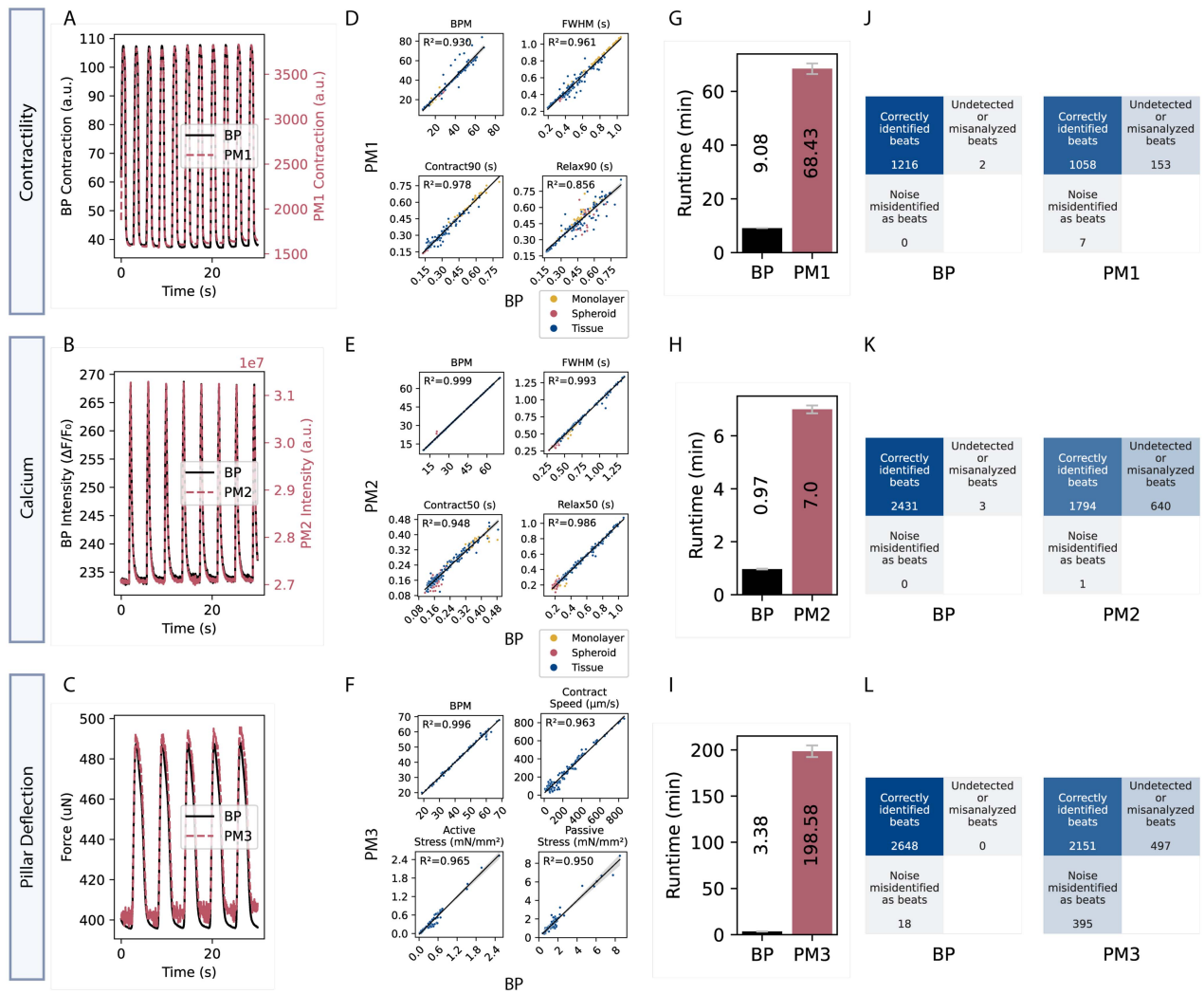
Fig. 3. Validation of BeatProfiler's extracted features (a) Representative contractile traces in monolayer from BeatProfiler (BP) and a previously published method (PM1). (b) Representative calcium traces in monolayer (BP and PM2). (c) Representative pillar deflection traces in milliPillar tissues (BP and PM3). (d) Pearson correlation between features extracted by BP and PM1 (n=40 for monolayers, n=19 for spheroids, n=118 for tissues). Clockwise from top left: beats per minute (BPM) ($p < 10^{-102}$), full-width half max (FWHM) ($p < 10^{-124}$), relax90 ($p < 10^{-74}$), contract90 ($p < 10^{-146}$). (e) Pearson correlation between features extracted by BP and PM2 (n=35 for monolayers, n=46 for spheroids, n=163 for tissues). Clockwise from top left: beats per minute (BPM) ($p < 10^{-307}$), full-width half max (FWHM) ($p < 10^{-264}$), relax50 ($p < 10^{-226}$), contract50 ($p < 10^{-157}$). (f Pearson correlation between features extracted from BP and PM3 (n=137 for tissues). Clockwise from top left: BPM ($p < 10^{-162}$), contraction speed ($p < 10^{-97}$), passive stress ($p < 10^{-88}$), active stress ($p < 10^{-99}$). (g) Functional video analysis time comparison (BP and PM1). 15 brightfield videos (5 monolayers, 5 spheroids, and 5 tissues) were measured 5 times. (h) Functional video analysis time comparison (BP and PM2). 15 calcium videos (5 monolayers, 5 spheroids, and 5 tissues) were measured 5 times (i) Functional video analysis time comparison (BP and PM3). 5 tissue videos were measured 5 times. (J to L) Confusion matrix indicating correctly identified beats, noise misidentified as beats (False positive), undetected or misanalyzed beats (False negative). (j) Contractility analysis accuracy matrix (48 monolayer, 32 spheroid, and 34 tissue videos). (k) Calcium analysis accuracy matrix from an aggregate of 48 monolayer videos, 37 spheroid videos, and 97 tissue videos. (l) Tissue pillar deflection analysis accuracy matrix (163 tissue videos).

B. Rapid Measurements of Contractile, Tissue Pillar Deflection, and Calcium Function in Correlation With Existing Standards

Comparative experiments were conducted to assess the versatility of BeatProfiler and benchmark its performance against previously published methods (PM 1–3) [4], [7], [9] for each functional modality: *contractility, calcium handling,* and *tissue pillar deflection.* The published methods were chosen based on the following criteria: 1) code and methodologies are described and documented online in a well cited publication, 2) software

is freely available to download at the time of this manuscript's publication.

To assess BeatProfiler's multimodal feature extraction, we compared BeatProfiler's contractility analysis to PM1, calcium analysis to PM2, and pillar deflection analysis to PM3 [4], [7], [9]. Representative traces from the three video modalities from BeatProfiler and existing methods are nearly congruent (Fig. 3(a)–(c). Metrics extracted from BeatProfiler show high correlations with those obtained by published methods using videos of different biological in vitro models, including monolayers, cardiac spheroids, and engineered tissues [4], [7], [9]

(Fig. 3(d)–(f), Fig. S4A-C). For this analysis, videos that failed to be properly analyzed by PM 1–3, but not BeatProfiler, were excluded from validation.

To assess the computational speed and robustness of Beat-Profiler, we compared its performance with existing methods [4], [7], [9] on the same computer. BeatProfiler performed more than seven times faster than previous methods in analyzing contractility and calcium modalities and over 50 times faster in analyzing pillar deflection in processing a set of test videos (Fig. 3(g)–(i).

We further validated BeatProfiler's accuracy and robustness by manually reviewing videos to assess misanalyzed/undetected beats and noise misidentified as beats. Unlike the previous comparison shown in Fig. 3(d)–(f), we included all videos in the analysis including those that failed to be properly analyzed by any given software. We determined that it reduced errors compared to existing methods (Fig. 3(j)–(l)). All methods performed well when the signal-to-noise ratio was high, but BeatProfiler was found to robustly analyze beats even when signals were suboptimal due to small contraction magnitudes or dim calcium fluorescent signals as further detailed in supplementary (Fig. S4D-I). BeatProfiler was especially useful in the pillar deflection modality due to its ability to robustly quantify subpixel level of contractions, a challenging feat that previous methods fail to quantify when tissues are exhibiting minute contractions imperceptible to the human eye.

C. Validation of BeatProfiler's Disease Phenotyping

We demonstrate the ability to detect functional changes accompanying disease. To demonstrate, we investigated restrictive cardiomyopathy resulting from a filamin C (*FLNC*) variant. BeatProfiler measured contractility, calcium transients, and tissue pillar deflection in iPS-CM monolayers and cardiac tissues engineered from these cells. Videos taken from a previously published dataset [24] were analyzed both with BeatProfiler and PM 1–3 to validate the accuracy of BeatProfiler. BeatProfiler identified phenotypic differences in all three modalities, and results were confirmed using PM 1–3. In congruence with previous findings, brightfield contractile analysis revealed impaired contraction and relaxation speeds, and calcium imaging revealed significant prolongation of tau and relax90 (Fig. 4(a) and (b), Fig. S5A-B), indicating impaired calcium handling resulting from the genetic mutation. In engineered tissues, decreased active force generation and increased passive tension also reflected a restrictive cardiomyopathy phenotype seen in previous studies (Fig. 4(c) and Fig. S5C) [24].

D. Validation of BeatProfiler's Detection of Dose-Dependent Drug Response

Analyzing drug response is of particular interest for drug discovery and drug safety assessment. Therefore, to assess BeatProfiler's ability to detect drug effects on cardiac function, iPS-CM response to isoproterenol, a β-adrenergic agonist with positive chronotropic effects, was analyzed at various concentrations. Dose-dependent functional changes were observed in engineered tissues for all three modalities, indicated by a positive relationship between concentration and beat frequency in addition to other temporal metrics (Fig. 4(d)–(f) and Fig. S5D-F). EC50 of isoproterenol was previously reported as 12.9 nM to 315 nM in stem cell derived cardiomyocytes [27], [28]. In contrast, the adult human ventricular cardiomyocytes exhibit an EC50 of 1.2 nM [29]. Our estimated EC50s of isoproterenol derived from each feature fall within this range in accordance with previously published data.

E. High-Throughput Profiling of Restrictive Cardiomyopathy and Feature-Based MI Classification

To demonstrate the capability of our pipeline for profiling disease phenotypes, we examined the spontaneous calcium response in a patient derived iPS-CM model of restrictive cardiomyopathy (FLNC$^{\Delta GAA}$) and its isogenic CRISPR-corrected control (FLNC$^{\Psi WT}$) using a high-throughput FLIPR assay from a previously published study [24] (Fig. 5(a)). We analyzed the time series traces using BeatProfiler, correcting for photobleaching, and found several functional differences among the twenty-five extracted features (Fig. 5(b)) in congruence with published data [24].

Using the twenty-five features extracted by BeatProfiler as input, ML models were trained to distinguish calcium responses of diseased and healthy cardiomyocytes. Among several feature-based ML models [30], [31], [32], [33], [34], [35], [36], SVC was identified as the best model based on its classification accuracy of 98.98% (Fig. 5(c) and (d)). Ranking the feature importance by linear SVC coefficient magnitudes revealed that the most critical feature associated with diseased cardiomyocytes was prolonged relax90, a metric of calcium decay duration in line with the impaired relaxation phenotype associated with restrictive cardiomyopathy [24] (Fig. 5(e)).

F. Automated Acquisition of Drug Response and Deep Learning Approaches to Classify Cardioactive Drugs

To illustrate another application of our pipeline, we acquired the calcium response of iPS-CM-GCaMP6f, a genetically encoded calcium indicator, to several cardioactive drugs with different properties using our customized automated acquisition system (Fig. S1). Quinidine, propranolol, E-4031, and verapamil were selected for their sodium channel, β-adrenergic, potassium channel, and calcium channel blocking effects, respectively. Calcium response to each drug is shown in a representative overlay of single-beat time series (Fig. 6(a)). Notably, quinidine and verapamil were associated with increased and decreased upstroke time, respectively, as measured by contract50 in line with previous findings (Fig. 6(b)) [37]. All drugs modulated tau, the time decay constant [38]. E-4031 was associated with increased RMSSD, a metric of interbeat variability, owing to its proarrhythmic potential [39].

Next, we sought to develop ML algorithms to classify drugs with different mechanisms of action. We explored several methods, from traditional feature-based ML to deep learning models that use raw traces as input. The best model, a custom-designed TCN-BiLSTM model (Fig. 6(c)) that takes a one-dimensional
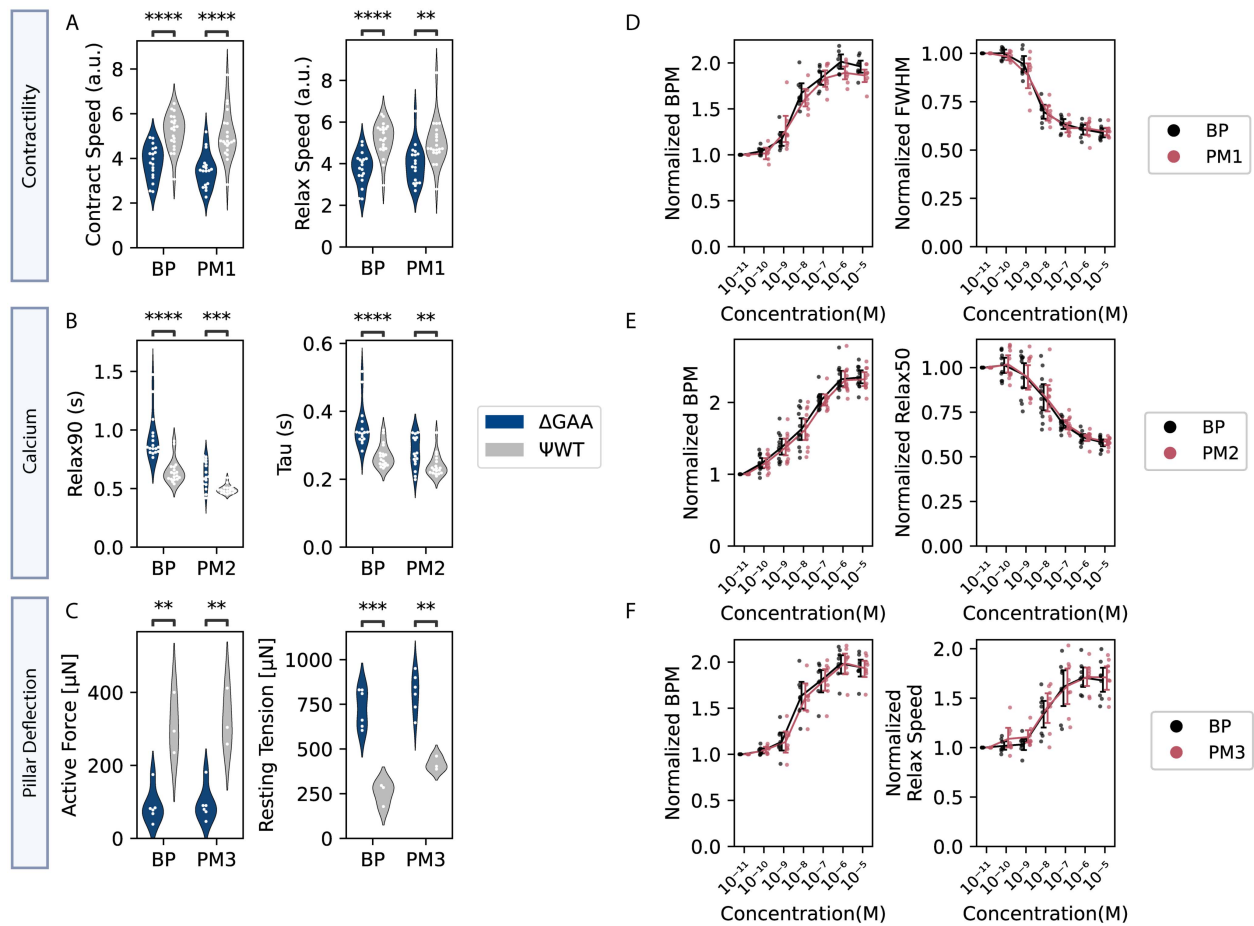
Fig. 4. Validation of BeatProfiler's capability to profile drugs and diseases (A to C) BeatProfiler identifies phenotypic differences between patient-derived iPS-CM (FLNC$^{\triangle GAA}$) and CRISPR-corrected iPS-CM (FLNC$^{\Psi WT}$) in congruence with existing methods. (a) Contraction (left) and relaxation speed (right) are impaired in patient-derived cardiomyocytes in contractile imaging of monolayers (n=36 for $\triangle$GAA, n=42 for ΨWT). (b) Relax90 (left) and tau (right) are increased in patient-derived cardiomyocytes in calcium imaging of monolayers (n=34 for $\triangle$GAA, n=36 for ΨWT). (c) Active force (left) generation is impaired, and passive tension (right) is increased in patient-derived cardiomyocytes in pillar tracking of engineered tissues (n=12 for $\triangle$GAA, n=6 for ΨWT). (D to F) BeatProfiler identifies dose-dependent isoproterenol drug response in engineered tissues in congruence with existing methods. Each tissue normalized to its values at 10^{-11}M. (d) Isoproterenol increases BPM (left; EC50 estimated by BP: 4.742 nM, EC50 estimated by PM1: 3.257 nM) and decreases FWHM (right; EC50 estimated by BP: 3.983 nM, EC50 estimated by PM1: 2.649 nM) in brightfield contractile imaging of tissues (n=8). (e) Isoproterenol increases BPM (left; EC50 estimated by BP: 13.76 nM, EC50 estimated by PM2: 12.99 nM) and decreases relax50 (right; EC50 estimated by BP: 19.11 nM, EC50 estimated by PM2: 15.83 nM) in calcium imaging of tissues (n=11). (f) Isoproterenol increases BPM (left; EC50 estimated by BP: 5.426 nM, EC50 estimated by PM3: 5.920 nM) and relaxation speed (right; EC50 estimated by BP: 10.99 nM, EC50 estimated by PM3: 9.130 nM) in brightfield pillar tracking of tissues (n=8).

time series as input, achieved an average accuracy of 96.25% (Fig. 6(d), Fig. S3A-D) and a weighted average F1 score of 0.9623 on the test set (Fig. 6(e), Table S6). In contrast, traditional feature-based approaches achieved only 45% to 79% accuracy. We also transformed our time series dataset into images to use as input to leverage widely available state-of-the-art image deep learning models. To expedite training and improve accuracy, we applied transfer learning by fine-tuning models pre-trained on ImageNet, a natural image dataset. This resulted in 2–5% increase in classification accuracy for each model. Image-based deep learning models performed better than feature-based models and were comparable to time series deep learning models with transfer learning.

To determine the optimal number of training samples required for high accuracy, we trained best-performing models for each input data type with a fraction of the total training dataset while fixing the validation and test sets. Namely, models tested were hybrid TCN-BiLSTM [40], [41] for time series input, SqueezeNet [42] with transfer learning and DenseNet [43] without transfer learning for GAF images, and random forest [35] for features. Feature-based ML had diminishing returns with more data, while deep learning approaches continued to improve with more data (Fig. S6A).

G. Deep Learning Model Interpretation Highlights Regions of Importance

We applied model interpretation methods to several drug classification models to better understand model decision-making processes. The best feature-based model, random forest, was interpreted by measuring the reduction in accuracy resulting from randomization of each feature one at a time. This allowed
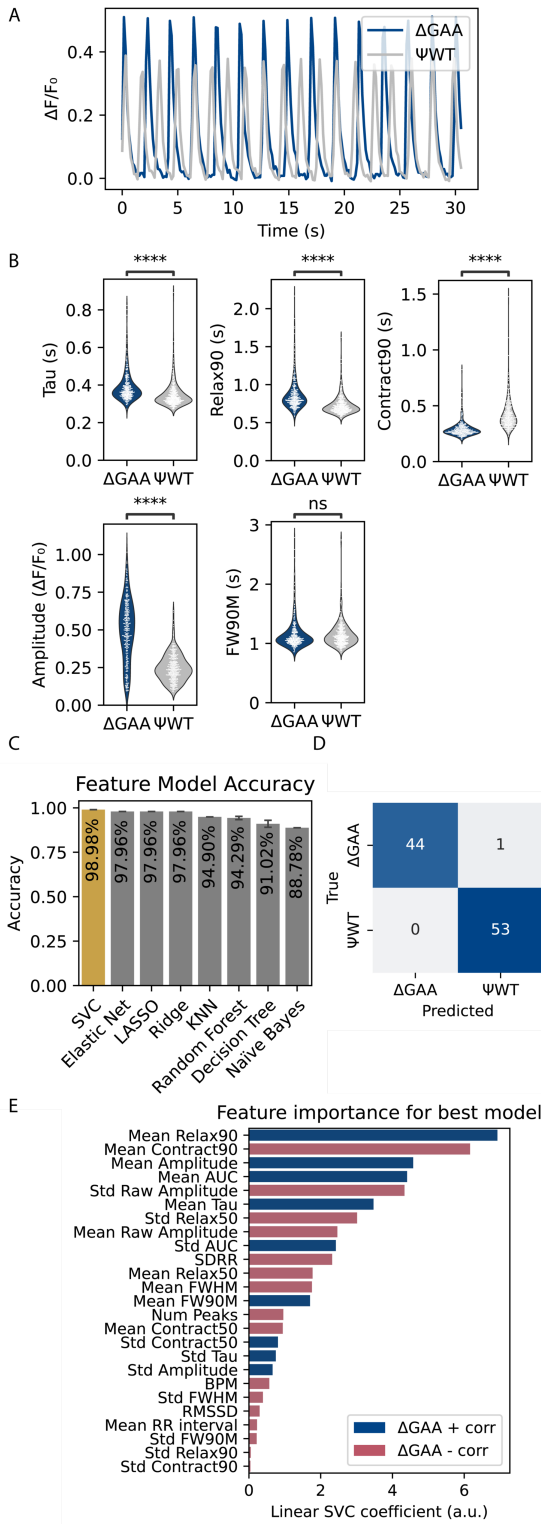
Fig. 5. Phenotyping restrictive cardiomyopathy with BeatProfiler (a) Representative calcium traces of GCaMP$^{\triangle GAA}$ and isogenic control GCaMP$^{\Psi WT}$ in monolayer. (b) GCaMP$^{\triangle GAA}$ is associated with increased tau, increased relax90, decreased contract90, increased amplitude, and no changes in FW90M in calcium imaging (n=352 for GCaMP$^{\Psi WT}$ and n=296 for GCaMP$^{\triangle GAA}$). (c) Classification accuracy of feature-based machine learning methods. (d) Confusion matrix of support vector classifier (SVC) classification model. (e) Feature importance for the SVC model.
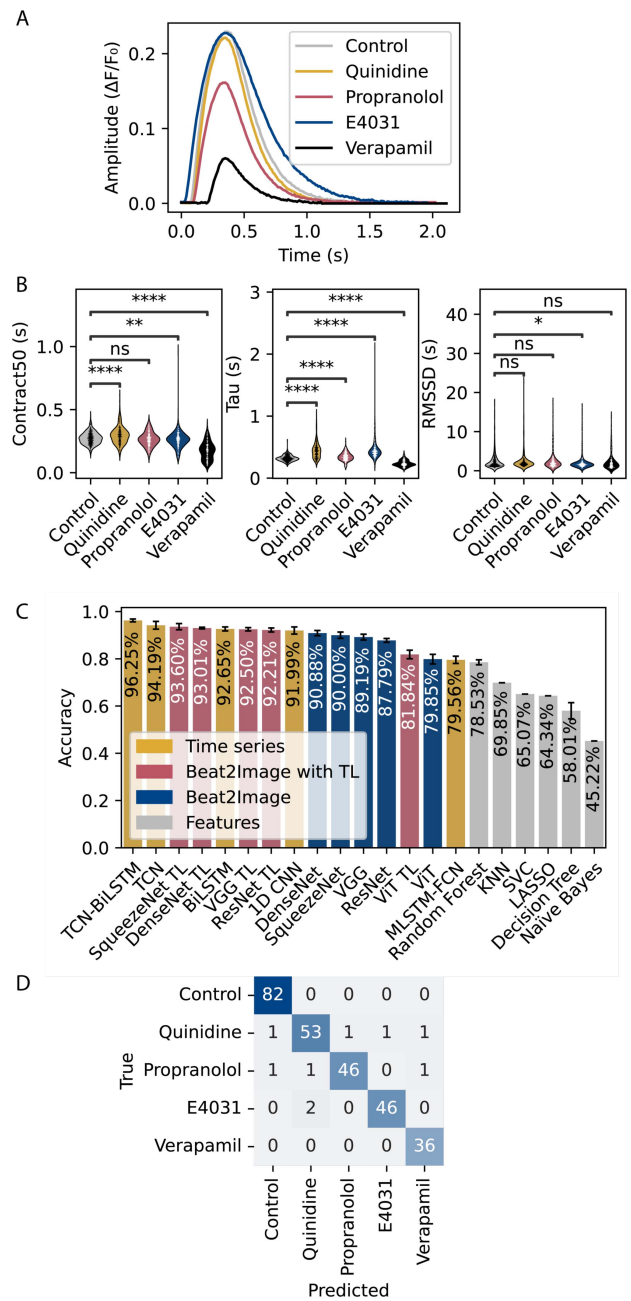

Fig. 6. Profiling cardioactive drug response with BeatProfiler (a) Representative calcium traces of iPS-CM perturbed with cardioactive drugs in monolayer. (b) Contract50 is increased by quinidine and decreased by E4031 and verapamil. Tau is increased by quinidine, propranolol, and E4031 and decreased by verapamil. RMSSD, a measure of interbeat variability, is increased in E4031, an arrhythmogenic drug. (544 samples for control, 376 samples for quinidine, 326 samples for propranolol, 319 samples for E-4031, and 243 samples for verapamil). (c) Model accuracy colored by input data types. (d) Confusion matrix of TCN-BiLSTM summarizing true/false positives and negatives.

us to rank the importance of each input feature in this model (Fig. S6B), revealing relax50, tau, standard deviation of FWHM, amplitude, and bpm as the five most important features.

Our best overall models were based on deep learning, so we turned to Grad-CAM to visualize regions of importance for
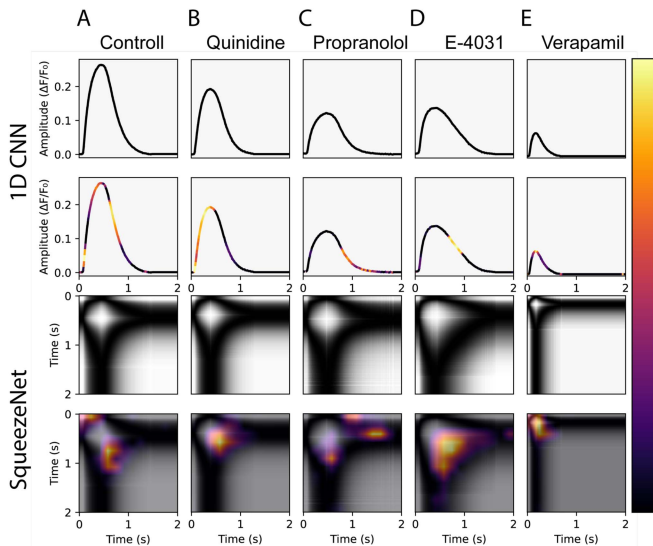
Fig. 7. Deep learning drug classification model interpretation through Grad-CAM. From top to bottom: calcium trace, trace with Grad-CAM heatmap highlighting region of importance in the 1D CNN model, input GAF image of the same trace, GAF highlighting region of importance in the SqueezeNet model with transfer learning. (a) Representative calcium trace of the no drug class. Multiple regions are highlighted in the time series. Upstroke and downstroke regions are highlighted in the GAF image. (b) Representative calcium trace of quinidine. The upstroke region is highlighted in the time series. Peak and downstroke regions are highlighted in the GAF image. (c) Representative calcium trace of propranolol. The latter downstroke region is highlighted in the time series. The latter downstroke region is highlighted in the GAF image. (d) Representative calcium trace of E-4031. The downstroke region is highlighted in the time series. The downstroke region is highlighted in the GAF image. (e) Representative calcium trace of verapamil. The peak region is highlighted in the time series. The peak region is highlighted in the GAF image.

specific examples. As Grad-CAM is only validated in convolution-based models, which TCN-BiLSTM is not, we applied it to the 1D CNN time series model and the CNN-based SqueezeNet image model with transfer learning instead, which had classification accuracy above 90%.

We show representative Grad-CAMs for each drug highlighting regions of importance for classification, visualizing the same sample in two models with different data representations. We identified unique patterns associated with each drug, reflecting each drug's unique perturbations of the cardiac cycle (Fig. 7). Grad-CAM enabled visualizations for regions of importance in the deep learning model decision-making process, reflecting a drug's effect in cardiomyocyte calcium response.

IV. DISCUSSION

There is a clear need for rapid and user-friendly software to reliably quantify in vitro cardiac function in multiple imaging modalities in applications to uncover cardiac disease phenotypes, unravel the underlying disease mechanisms, and detect cardioactive drug effects. However, there is currently a lack of user-friendly tools for rapid and unbiased analysis of this kind. BeatProfiler provides fast and robust cardiac contractile and calcium function analysis in monolayers, spheroids, and engineered tissues.

Available at beatprofiler.github.io along with documentations, example data, and tutorials, the Windows and macOS-compatible GUI was developed in Python and PySide2 as a standalone software, enabling users to download a single installer without additional setup. Furthermore, BeatProfiler's speed improvements enable true real-time monitoring through simultaneous video acquisition and analysis. Specifically designed for high throughput experiments, BeatProfiler enables analysis of thousands of samples at once. BeatProfiler's strength lies in its versatility and customizability while keeping the GUI simple and easy to use. In addition, advanced users can use the Python library to customize analysis to fit their needs. Paired with our automated acquisition program and ML algorithms, BeatProfiler enables high-throughput experiments and analysis on a standard microscope and computer system.

BeatProfiler was validated for reliably detecting functional perturbations due to disease and drugs. In congruence with previous findings, pathogenic RCM iPS-CM monolayers showed prolonged contraction and relaxation velocity in contractility imaging and prolonged tau in calcium imaging indicating impaired relaxation. Restrictive phenotype was observed in engineered tissues through impaired active force generation and increased resting tension. BeatProfiler also quantified dose-dependent positive chronotropic response to β-adrenergic agonist isoproterenol in various functional metrics derived from contractility imaging, tissue pillar tracking, and calcium imaging, thereby confirming BeatProfiler's ability to robustly detect drug-induced changes in cardiac function.

As cardiotoxicity is a major cause for concern in drug development, BeatProfiler is designed to extract key metrics that are crucial for evaluating cardiotoxic potential. Specifically, it quantifies interbeat variability through metrics such as Standard Deviation of RR intervals (SDRR) and Root Mean Square of Successive Differences (RMSSD). These metrics are valuable for flagging compounds with potential cardiotoxic effects, as increased variability can be indicative of cardiac stress or dysfunction. Additionally, BeatProfiler can assess the risk of prolonged QT intervals by measuring changes in tau. Although our study did not focus on fluorescent voltage indicators, it's pertinent to note that BeatProfiler is also capable of analyzing action potential duration (APD90) from voltage data. This is particularly relevant for detecting drugs that may cause prolonged action potential duration, a known risk factor for cardiotoxicity. By leveraging these capabilities, BeatProfiler presents a versatile tool for early detection of cardiotoxicity, thereby aiding in the safer development of new pharmaceutical compounds.

We demonstrated several applications for using BeatProfiler, one of which was to pinpoint disease phenotypes associated with a restrictive cardiomyopathy-associated gene using ML. We illustrate that BeatProfiler easily integrates into existing pipelines, such as a FLIPR assay, to extract relevant features. In line with previous findings, the most distinctive feature of $GCaMP^{\Delta GAA}$ compared to $GCaMP^{\Psi WT}$ identified in the calcium transient was increased relax90. This rapid quantification of cardiac function and ML classification could be applied to detect functional changes brought on by novel mutations or variants of uncertain significance in a high-throughput manner.

We also investigated cardioactive drug responses of iPS-CMs acquired by our automated imaging pipeline to demonstrate ML-based identification of cardioactivity by mechanism of action. Like the previous application, we applied feature-based ML but instead found limitations in traditional models, especially in classifying quinidine, propranolol, and E-4031 likely due to the indiscriminate nature of these blockers. Several drugs have secondary blocking effects that overlap with each other. Quinidine is a Na-blocker also known to have K-blocking effects. Propranolol is a β-blocker with Na-blocking effects.

To tackle the limitation of feature-based models, we applied deep learning approaches to achieve higher classification performance through a different input representation to extract information not fully captured in predetermined features. While deep learning models are burdened by reduced explainability and increased computational resources, advancements in explainable AI such as Grad-CAM, increase in GPU computing power, and a decrease in computing cost in recent years have made this approach more viable. We explored TCN and Bi-LSTM as these methods have proven successful in other temporal datasets [44], [45], [46], [47], [48]. TCN and BiLSTM performed well at 94.12% and 92.65% average accuracy, respectively. Our best model, a hybrid model with both TCN and BiLSTM components, achieved 96.25% average accuracy, suggesting that a synergistic effect of feature extraction and improved modeling of complex temporal dependencies increased the accuracy.

While our customized TCN-BiLSTM model, which takes time series beats as input, performed the best, we wanted to demonstrate that existing models could also achieve good results by non-ML experts. Image classification models widely available through resources such as PyTorch, TensorFlow, and fastai require just a few lines of code [49], [50], [51], which motivated us to add an image transformation feature to BeatProfiler to help democratize and maximize potential downstream applications with deep learning.

We show comparable results of our best-performing models with several popular image models without any modifications. Networks pre-trained on the ImageNet dataset were fine-tuned to improve the classification significantly. Our best image models with transfer learning achieved accuracies nearly as high as our best overall model within just 3–4%.

To identify which calcium trace region is uniquely perturbed for each drug, we applied Grad-CAM, a technique developed for deep learning networks based on convolution, to highlight regions of importance in classification. We show representative samples for each drug type by applying Grad-CAM to two convolution-based models (1D-CNN for time series and SqueezeNet with transfer learning for image). Due to the limitation of this method that restricts its usage to only convolution-based models, we could not apply it to our best-performing model, TCN-BiLSTM. Interestingly, we noticed several parallels in highlighted regions with known perturbations in cardiac action potentials [52]. Decrease in depolarization slope characterizes a class IA Na-blocker. The quinidine trace showing a highlighted upstroke may suggest Na-blocking may also perturb that part of the calcium transient. Propranolol trace exhibits a highlighted area near the end of the trace, alluding to effects of increased refractory period between beats. The E-4031 trace

highlights the downstroke, congruent with known prolonged repolarization effects of a K-blocker. The calcium-blocker trace highlights the peak of the trace, indicating its impact on the trace amplitude. Lastly, the control trace is highlighted in many regions likely to rule out other possibilities during decision-making. While we used Grad-CAM as means for validation using well known drugs, this suggests it can infer insight into previously unknown drugs in drug development. BeatProfiler, combined with the deep learning classification and interpretation methods described, could help profile cardiac function in the drug development pipeline to detect and identify the type of cardioactivity. Additional future directions and limitations for this study are described in supplementary materials.

V. CONCLUSION

In summary, this study demonstrates capabilities of the all-in-one analysis tool BeatProfiler in many modalities ranging from contractility, calcium fluorescence, and uniaxial tissue pillar deflection. BeatProfiler GUI enables easy, rapid, and accurate identification of disease phenotypes and drug effects for multiple biological models (monolayers, spheroids, engineered tissues) and is available at beatprofiler.github.io. Furthermore, we illustrate that ML applications and their interpretations can predict and profile cardiac function. We foresee that BeatProfiler, the automated data acquisition pipeline, and ML methods described here will help advance in vitro cardiac functional assessment, reveal complex mechanisms in disease, and accelerate drug discovery.

SUPPLEMENTARY MATERIALS

Supplementary materials include cell culture methods, dataset details for BeatProfiler validation, experimental details for the drug study, data acquisition methods, ML train/test splits, and ML model architectures for drug and disease classification. Detailed information about BeatProfiler analysis pipeline, improvements of BeatProfiler from existing methods, and limitations of BeatProfiler are also outlined.

AUTHORS CONRTRIBUTIONS

Y.K., K.W., B.M.F., and G.V.N. wrote and edited the manuscript. Y.K., K.W., and G.V.N. designed the experiments. Y.K., K.W., R.I.L., T.R.N., S.F., B.Z.W. performed the experiments. Y.K. and K.W. developed the software, analyzed the data, and interpreted the results. All authors reviewed the manuscript.

CONFLICT OF INTEREST

The authors declare no conflict of interest related to the work reported in this article.

ACKNOWLEDGMENT

their experimental data and for their inputs that helped us make BeatProfiler more user-friendly. Graphical figures were created with BioRender.com.

REFERENCES

[1] D. A. Eisner, J. L. Caldwell, K. Kistamás, and A. W. Trafford, "Calcium and excitation-contraction coupling in the heart," *Circ. Res.*, vol. 121, no. 2, pp. 181–195, Jul. 2017, doi: 10.1161/CIRCRESAHA.117.310230.

[2] D. M. Bers, "Cardiac excitation–contraction coupling," *Nature*, vol. 415, no. 6868, pp. 198–205, Jan. 2002, doi: 10.1038/415198a.

[3] A. J. S. Ribeiro et al., "Considerations for an In vitro, cell-based testing platform for detection of drug-induced inotropic effects in early drug development. Part 2: Designing and fabricating microsystems for assaying cardiac contractility with physiological relevance using Human iPSC-cardiomyocytes," *Front. Pharmacol.*, vol. 10, Aug. 2019, Art. no. 934, doi: 10.3389/fphar.2019.00934.

[4] L. Sala et al., "MUSCLEMOTION: A versatile open software tool to quantify cardiomyocyte and cardiac muscle contraction In vitro and In vivo," *Circ. Res.*, vol. 122, no. 3, pp. e5–e16, Feb. 2018, doi: 10.1161/CIRCRESAHA.117.312067.

[5] T. Hayakawa et al., "Image-based evaluation of contraction–relaxation kinetics of human-induced pluripotent stem cell-derived cardiomyocytes: Correlation and complementarity with extracellular electrophysiology," *J. Mol. Cell. Cardiol.*, vol. 77, pp. 178–191, Dec. 2014, doi: 10.1016/j.yjmcc.2014.09.010.

[6] A. Ahola, A. L. Kiviaho, K. Larsson, M. Honkanen, K. Aalto-Setälä, and J. Hyttinen, "Video image-based analysis of single human induced pluripotent stem cell derived cardiomyocyte beating dynamics using digital image correlation," *Biomed. Eng. OnLine*, vol. 13, no. 1, Apr. 2014, Art. no. 39, doi: 10.1186/1475-925X-13-39.

[7] Y. Psaras et al., "CalTrack: High-throughput automated calcium transient analysis in cardiomyocytes," *Circ. Res.*, vol. 129, no. 2, pp. 326–341, Jul. 2021, doi: 10.1161/CIRCRESAHA.121.318868.

[8] F. Cerignoli et al., "High throughput measurement of Ca2+ dynamics for drug risk assessment in Human stem cell-derived cardiomyocytes by kinetic image cytometry," *J. Pharmacol. Toxicol. Methods*, vol. 66, no. 3, pp. 246–256, 2012, doi: 10.1016/j.vascn.2012.08.167.

[9] M. A. Tamargo et al., "milliPillar: A platform for the generation and real-time assessment of human engineered cardiac tissues," *ACS Biomater. Sci. Eng.*, vol. 7, no. 11, pp. 5215–5229, Nov. 2021, doi: 10.1021/acsbiomaterials.1c01006.

[10] J. M. Rivera-Arbeláez et al., "Automated assessment of human engineered heart tissues using deep learning and template matching for segmentation and tracking," *Bioeng. Transl. Med.*, vol. 8, no. 3, Apr. 2023, Art. no. e10513, doi: 10.1002/btm2.10513.

[11] H. Vandenburgh et al., "Drug-screening platform based on the contractility of tissue-engineered muscle," *Muscle Nerve*, vol. 37, no. 4, pp. 438–447, 2008, doi: 10.1002/mus.20931.

[12] S. Dara, S. Dhamercherla, S. S. Jadav, C. M. Babu, and M. J. Ahsan, "Machine learning in drug discovery: A review," *Artif. Intell. Rev.*, vol. 55, no. 3, pp. 1947–1999, 2022, doi: 10.1007/s10462-021-10058-4.

[13] D. Ardila et al., "End-to-end lung cancer screening with three-dimensional deep learning on low-dose chest computed tomography," *Nature Med.*, vol. 25, no. 6, Jun. 2019, Art. no. 6, doi: 10.1038/s41591-019-0447-x.

[14] L. McInnes, J. Healy, N. Saul, and L. Großberger, "UMAP: Uniform Manifold approximation and projection," *J. Open Source Softw.*, vol. 3, no. 29, Sep. 2018, Art. no. 861, doi: 10.21105/joss.00861.

[15] N. J. Bernstein, N. L. Fong, I. Lam, M. A. Roy, D. G. Hendrickson, and D. R. Kelley, "Solo: Doublet identification in single-cell RNA-seq via semi-supervised deep learning," *Cell Syst.*, vol. 11, no. 1, pp. 95–101, Jul. 2020, doi: 10.1016/j.cels.2020.05.010.

[16] A. Strokach, D. Becerra, C. Corbi-Verge, A. Perez-Riba, and P. M. Kim, "Fast and flexible protein design using deep graph neural networks," *Cell Syst.*, vol. 11, no. 4, pp. 402–411, Oct. 2020, doi: 10.1016/j.cels.2020.08.016.

[17] B. Hie, B. D. Bryson, and B. Berger, "Leveraging uncertainty in machine learning accelerates biological discovery and design," *Cell Syst.*, vol. 11, no. 5, pp. 461–477, Nov. 2020, doi: 10.1016/j.cels.2020.09.007.

[18] D. Teles, Y. Kim, K. Ronaldson-Bouchard, and G. Vunjak-Novakovic, "Machine learning techniques to classify healthy and diseased cardiomyocytes by contractility profile," *ACS Biomater. Sci. Eng.*, vol. 7, no. 7, pp. 3043–3052, Jul. 2021, doi: 10.1021/acsbiomaterials.1c00418.

[19] M. Juhola, H. Joutsijoki, K. Penttinen, and K. Aalto-Setälä, "Detection of genetic cardiac diseases by Ca^{2+} transient profiles using machine learning methods," *Sci. Rep.*, vol. 8, no. 1, Jun. 2018, Art. no. 1, doi: 10.1038/s41598-018-27695-5.

[20] M. Juhola, H. Joutsijoki, K. Penttinen, and K. Aalto-Setälä, "Machine learning to differentiate diseased cardiomyocytes from healthy control cells," *Inform. Med. Unlocked*, vol. 14, pp. 15–22, Jan. 2019, doi: 10.1016/j.imu.2019.01.006.

[21] E. K. Lee et al., "Machine learning of Human pluripotent stem cell-derived engineered cardiac tissue contractility for automated drug classification," *Stem Cell Rep.*, vol. 9, no. 5, pp. 1560–1572, Nov. 2017, doi: 10.1016/j.stemcr.2017.09.008.

[22] C. Heylman, R. Datta, A. Sobrino, S. George, and E. Gratton, "Supervised machine learning for classification of the electrophysiological effects of chronotropic drugs on human induced pluripotent stem cell-derived cardiomyocytes," *PLoS One*, vol. 10, no. 12, Dec. 2015, Art. no. e0144572, doi: 10.1371/journal.pone.0144572.

[23] P. Aghasafari et al., "A deep learning algorithm to translate and classify cardiac electrophysiology," *eLife*, vol. 10, Jul. 2021, Art. no. e68335, doi: 10.7554/eLife.68335.

[24] B. Z. Wang et al., "Engineered cardiac tissue model of restrictive cardiomyopathy for drug discovery," *Cell Rep. Med.*, vol. 4, no. 3, Mar. 2023, Art. no. 100976, doi: 10.1016/j.xcrm.2023.100976.

[25] G. Jocher, A. Chaurasia, and J. Qiu, "Ultralytics YOLOv8," 2023. [Online]. Available: https://docs.ultralytics.com/models/yolov8/?h=cit#_tabbed_3_1

[26] B. D. Lucas and T. Kanade, "An iterative image registration technique with an application to stereo vision," in *Proc. IJCAI'81: 7th Int. joint Conf. Artif. Intell.*, 1981, Art. no. 674. Accessed: Apr. 27, 2023. [Online]. Available: https://hal.science/hal-03697340

[27] M. Brito-Martins, S. E. Harding, and N. N. Ali, "β1- and β2-adrenoceptor responses in cardiomyocytes derived from human embryonic stem cells: Comparison with failing and non-failing adult human heart," *Brit. J. Pharmacol.*, vol. 153, no. 4, pp. 751–759, Feb. 2008, doi: 10.1038/sj.bjp.0707619.

[28] A. Mathur et al., "Human iPSC-based cardiac microphysiological system for drug screening applications," *Sci. Rep.*, vol. 5, Mar. 2015, Art. no. 8883, doi: 10.1038/srep08883.

[29] S. E. Harding, N. N. Ali, M. Brito-Martins, and J. Gorelik, "The human embryonic stem cell-derived cardiomyocyte as a pharmacological model," *Pharmacol. Ther.*, vol. 113, no. 2, pp. 341–353, Feb. 2007, doi: 10.1016/j.pharmthera.2006.08.008.

[30] C. Cortes and V. Vapnik, "Support-vector networks," *Mach. Learn.*, vol. 20, no. 3, pp. 273–297, Sep. 1995, doi: 10.1007/BF00994018.

[31] T. Cover and P. Hart, "Nearest neighbor pattern classification," *IEEE Trans. Inf. Theory*, vol. 13, no. 1, pp. 21–27, Jan. 1967, doi: 10.1109/TIT.1967.1053964.

[32] R. Tibshirani, "Regression shrinkage and selection via the lasso," *J. Roy. Statist. Soc. Ser. B Methodol.*, vol. 58, no. 1, pp. 267–288, 1996.

[33] A. E. Hoerl and R. W. Kennard, "Ridge regression: Biased estimation for nonorthogonal problems," *Technometrics*, vol. 42, no. 1, pp. 80–86, Feb. 2000.

[34] H. Zou and T. Hastie, "Regularization and variable selection via the elastic net," *J. Roy. Statist. Soc. Ser. B Statist. Methodol.*, vol. 67, no. 2, pp. 301–320, 2005.

[35] L. Breiman, "Random forests," *Mach. Learn.*, vol. 45, no. 1, pp. 5–32, Oct. 2001, doi: 10.1023/A:1010933404324.

[36] J. R. Quinlan, "Induction of decision trees," *Mach. Learn.*, vol. 1, no. 1, pp. 81–106, Mar. 1986, doi: 10.1007/BF00116251.

[37] F. Fuchs, E. W. Gertz, and F. N. Briggs, "The effect of quinidine on calcium accumulation by isolated sarcoplasmic reticulum of skeletal and cardiac muscle," *J. Gen. Physiol.*, vol. 52, no. 6, pp. 955–968, Dec. 1968.

[38] H. R. Lu et al., "High throughput measurement of Ca^{++} dynamics in Human stem cell-derived cardiomyocytes by kinetic image cytometry: A cardiac risk assessment characterization using a large panel of cardioactive and inactive compounds," *Toxicol. Sci.*, vol. 148, no. 2, pp. 503–516, Dec. 2015, doi: 10.1093/toxsci/kfv201.

[39] K. Harris, M. Aylott, Y. Cui, J. B. Louttit, N. C. McMahon, and A. Sridhar, "Comparison of electrophysiological data from human-induced pluripotent stem cell–Derived cardiomyocytes to functional preclinical safety assays," *Toxicol. Sci.*, vol. 134, no. 2, pp. 412–426, Aug. 2013, doi: 10.1093/toxsci/kft113.

[40] C. Lea, R. Vidal, A. Reiter, and G. D. Hager, "Temporal convolutional networks: A unified approach to action segmentation," in *Proc. Comput. Vis. ECCV Workshops*, 2016, pp. 47–54.

[41] S. Hochreiter and J. Schmidhuber, "Long short-term memory," *Neural Comput.*, vol. 9, no. 8, pp. 1735–1780, Nov. 1997, doi: 10.1162/neco.1997.9.8.1735.

[42] F. N. Iandola, S. Han, M. W. Moskewicz, K. Ashraf, W. J. Dally, and K. Keutzer, "SqueezeNet: AlexNet-level accuracy with 50x fewer parameters and <0.5MB model size," Nov. 2016, doi: 10.48550/arXiv.1602.07360.

[43] G. Huang, Z. Liu, L. van der Maaten, and K. Q. Weinberger, "Densely connected convolutional networks," in *Proc. IEEE Conf. Comput. Vis. Pattern Recognit.*, 2018, pp. 2261–2269, doi: 10.48550/arXiv.1608.06993.

[44] T. Thireou and M. Reczko, "Bidirectional long short-term memory networks for predicting the subcellular localization of eukaryotic proteins," *IEEE/ACM Trans. Comput. Biol. Bioinform.*, vol. 4, no. 3, pp. 441–446, Jul. 2007, doi: 10.1109/tcbb.2007.1015.

[45] T. M. Ingolfsson, X. Wang, M. Hersche, A. Burrello, L. Cavigelli, and L. Benini, "ECG-TCN: Wearable cardiac arrhythmia detection with a temporal convolutional network," in *Proc. IEEE 3rd Int. Conf. Artif. Intell. Circuits Syst.*, 2021, pp. 1–4. doi: 10.1109/AICAS51828.2021.9458520.

[46] C. Kok et al., "Automated prediction of sepsis using temporal convolutional network," *Comput. Biol. Med.*, vol. 127, Dec. 2020, Art. no. 103957, doi: 10.1016/j.compbiomed.2020.103957.

[47] J. Gao, H. Zhang, P. Lu, and Z. Wang, "An effective LSTM recurrent network to detect arrhythmia on imbalanced ECG dataset," *J. Healthcare Eng.*, vol. 2019, Oct. 2019, Art. no. 6320651, doi: 10.1155/2019/6320651.

[48] M. Schuster and K. Paliwal, "Bidirectional recurrent neural networks," *IEEE Trans. Signal Process.*, vol. 45, no. 11, pp. 2673–2681, Nov. 1997, doi: 10.1109/78.650093.

[49] A. Paszke et al., "PyTorch: An imperative style, high-performance deep learning library," in *Proc. Adv. Neural Inf. Process. Syst.*, Curran Associates, 2019, pp. 8026–8037. Accessed: Apr. 25, 2023. [Online]. Available: https://proceedings.neurips.cc/paper_files/paper/2019/hash/bdbca288fee7f92f2bfa9f7012727740-Abstract.html

[50] M. Abadi et al., "TensorFlow: A system for large-scale machine learning," in *Proc. 12th USENIX Symp. Operating Syst. Des. Implementation*, 2016, pp. 265–283. Accessed: Apr. 25, 2023, [Online]. Available: https://www.usenix.org/system/files/conference/osdi16/osdi16-abadi.pdf

[51] J. Howard and S. Gugger, "Fastai: A layered API for deep learning," *Information*, vol. 11, no. 2, Feb. 2020, Art. no. 108, doi: 10.3390/info11020108.

[52] A. O. Grant, "Cardiac ion channels," *Circ. Arrhythm. Electrophysiol.*, vol. 2, no. 2, pp. 185–194, Apr. 2009, doi: 10.1161/CIRCEP.108.789081.